Leveraging Halogen Interactions for a Supramolecular Nanotube

Sergey Fisher,[a,b] Lorraine A. Malaspina,[b] Cristian Gozálves Martinez,[c] Alessandro Prescimone,[c] Yaser Balmohammadi,[b] Simon Grabowsky,[b] and Tomáš Šolomek*[a]

Supramolcular nanotubes in a single crystal were produced from halogenated macrocycles by balancing hydrogen bonds and halogen interactions. A new iodinated macrocycle was prepared, crystallized, and a bonding analysis was performed to evaluate the nature and strength of the involved type I I···I interactions and C=O···I halogen bonds.

Tubular architectures are found in naturally occurring structures such as DNA[1], lipid membranes[2,3], and also in viruses, such as the tobacco mosaic virus[4]. Scientists have developed artificial tubular assemblies to uncover the mechanisms of the formation of these unique structures and to exploit them in materials sciences and biomimetic chemistry using macromolecular compounds.[5–11] Supramolecular tubules made of macrocycles offer numerous advantages, such as late-stage derivatization of individual monomers and the ability to form and tune their solid-state structures in crystals.[12–14] Stoddard and co-workers reported tubular self-assemblies of molecular triangles[15,16] and squares[17] made of naphthalene diimide (NDI). These structures exhibit a complex hydrogen bonding (HB) network which can easily lead to a mismatch between the donor and acceptor binding sites.[15] Nevertheless, the growth of tubular assemblies of **Δ-NDI** (Fig. 1) could be directed by type I halogen···halogen (X···X) interactions *between solvent molecules* trapped within the coaxial supramolecular channel.[16] In this case, however, the high boiling solvents block the intrinsic pore. To avoid blocking the pore, an alternative strategy independent of the solvent confined to the co-axial channels is needed.

Substitution of the NDIs by pyromellitic diimides (PMDIs) could allow for a linear elongation perpendicular to the macrocycle plane using halogen bonding (XB, Fig. 1). Indeed, halogenated PMDIs can form linear assemblies via intermolecular C=O···X (X = Br, I) XB in the solid state,[18,19] as supported by the crystal structure of 3,6-diiodo pyromellitic dianhydride (Fig. S11).

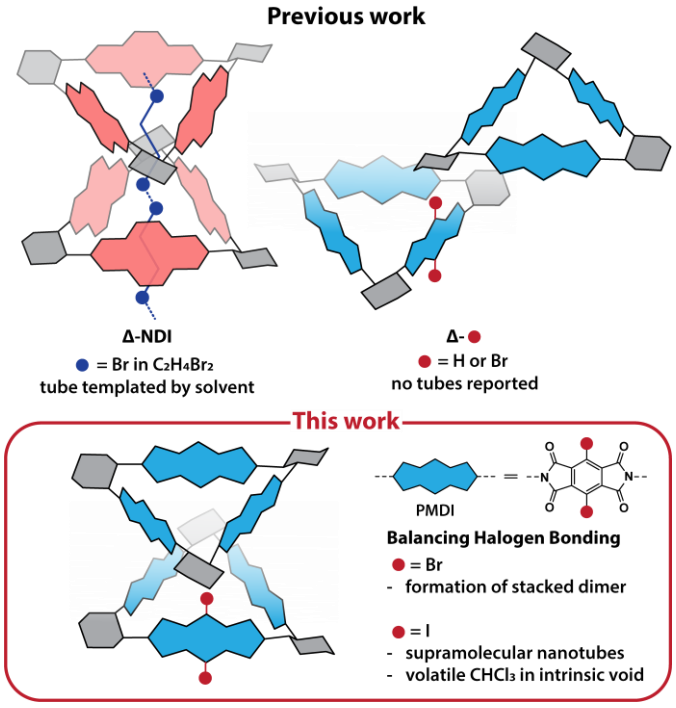

Fig. 1 Schematic supramolecular assemblies of **Δ-NDI** (top left) and **Δ-H** or **Δ-Br** (top right) macrocycles in the solid state and the SC-XRD structure of the iodinated macrocycle **Δ-I**.

In 2002, Gawroński and co-workers reported the first PMDI molecular triangles (**Δ-H**) that exhibited HB between the macrocycles. However, due to the non-linear nature of the HB interactions, a tubular assembly was not formed.[20] Recently, Zhao *et al.* incorporated bromine atoms into PMDIs, however, the resulting **Δ-Br** crystallized from THF (Fig. 2a) provided a hexagonal honeycomb superstructure directed exclusively by HB of C=O···H–C_{Cy} and Br···H–C_{Cy} type (Table S4).[21]

In this work, we achieve the formation of tubular supramolecular assemblies of halogenated PMDI molecular triangles in the solid state for the first time by systematically balancing the competing HB and the XB interactions (Fig. 1).

[a] *Van 't Hoff Institute for Molecular Sciences, University of Amsterdam, Science Park 904, NL-1098 XH Amsterdam, The Netherlands. E-mail: t.solomek@uva.nl.*
[b] *Department of Chemistry, Biochemistry and Pharmaceutical Sciences, University of Bern, Freiestrasse 3, CH-3012 Bern, Switzerland.*
[c] *Department of Chemistry, University of Basel, St. Johanns-Ring 19, CH-4056 Basel, Switzerland.*
† Footnotes relating to the title and/or authors should appear here.
Electronic Supplementary Information (ESI) available: [details of any supplementary information available should be included here]. See DOI: 10.1039/x0xx00000x

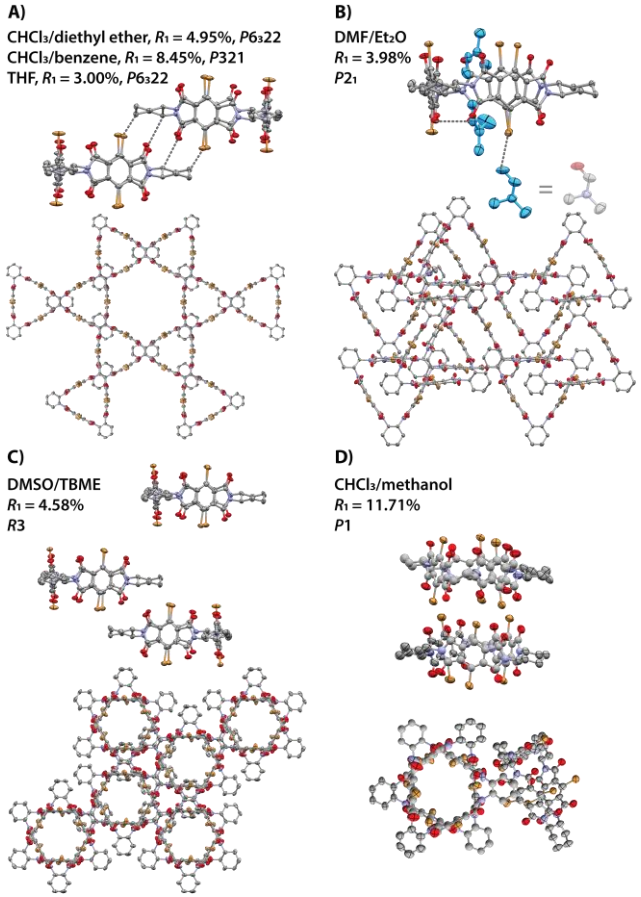

Fig. 2 SC-XRD structures of **Δ-Br** obtained from different solvents to steer the type of the solid-state assembly. Color code: C, grey; O, red; N, blue; Br, orange, Cl, green. Ellipsoids are shown at 50% probability and H and solvent molecules are omitted for clarity.

We first explored whether the HB donating/accepting character of the crystallization solvent could aid disrupting HB and reinforcing XB to achieve the tubular assembly of **Δ-Br**. We replaced THF (β = 0.55[22]) for a stronger HB acceptor *N*,*N*-dimethyl formamide (DMF, β = 0.71[22]). The solvent/antisolvent DMF/diethyl ether combination yielded a modification where two carbonyl oxygen atoms coordinate to the amide proton of DMF (Fig. 2B). A second DMF molecule was found in proximity to the bromine substituent, indicating a XB interaction. Utilizing the solvent mixture of dimethyl sulfoxide (DMSO, β_{DMSO} = 0.74[22])/methyl *tert*-butyl ether (TBME) resulted in a densely packed crystal structure directed by HB and Br···π close contacts showing that acidic protons are necessary to disrupt the HB bonds (Fig. 2C). We further tested $CHCl_3$ that cannot disrupt potential XB between two **Δ-Br** and which is a weak HB donor (α = 0.23[23]). $CHCl_3$/benzene and $CHCl_3$/Et_2O mixtures, however, did not affect the hexagonal honeycomb crystal morphology (Fig. 2A), although incorporation of benzene molecules in the crystal structure induced an unusual modulation and lowered the symmetry of the unit cell. We were partially successful when the single crystal was grown by slow evaporation of neat $CHCl_3$ (Fig. 2D). Here, we observed that a **Δ-Br** dimer was formed. Unfortunately, we were no able to obtain an unambiguous solution for this structure because the crystal turned amorphous within a few hours after being removed from the crystallization solvent. Nevertheless, this result suggested that XB could be leveraged to induce the formation of a supramolecular nanotube. Therefore, we switched to a more HB-active $CHCl_3$/methanol solvent mixture aiming at further disrupting the weak HB between **Δ-Br** by MeOH at the early stages of the crystal growth. Note that MeOH molecules do not incorporate in the crystal structures of macrocycles made of PMDIs or related rylene diimides.[24–26] We obtained a single crystal with complex unit cell consisting of four **Δ-Br** and 22 $CHCl_3$ molecules (Fig. 2D). However, we could not observe formation of a **Δ-Br** assembly longer than the dimer. Consequently, we decided to replace the bromine atoms by iodine atoms to further balance the interactions between the macrocycles: 1) the longer C–I bond should lengthen and thus weaken the C=O···H–C_{Cy} and X···H–C_{Cy} HBs, while 2) the larger σ-hole of iodine should strengthen the XB.

The synthesis of the iodinated PMDI macrocycle (**Δ-I**) was achieved by condensation of 3,6-diiodopyromellitic dianhydride and (1*R*,2*R*)-cyclohexane diamine. We obtained single crystals by benzene vapour diffusion into a saturated $CHCl_3$ solution. A single-crystal X-ray diffraction (SC-XRD) analysis showed that **Δ-I** crystallizes in the triclinic space group (*P*1, *a*=17.1608(3) Å, *b*=17.1753(2) Å, *c*=17.490(2) Å, α=87.816(1)°, β=86.388(1)°, γ=60.580(1)°; see SI, Table S1 for additional details), and the unit cell contains two **Δ-I** and fourteen benzene molecules (Fig. 3). Six benzene molecules coordinate to the electron-poor π-surface of the PMDIs, while the rest occupy the free space. The two **Δ-I** molecules are positioned above each other and displaced by 60°. The analysis of the solid-state superstructure reveals formation of the desired tubular architecture, possibly directed by XB interactions (see bonding analysis below). The individual supramolecular nanotubes are well-separated with a $C_{cy}(–H_2)\cdots C_{cy}(–H_2)$ distance of 3.72 Å indicating a negligible interaction between them. The disordered contents of the cavity within individual macrocycles could not be satisfactorily modelled, therefore, the contribution of 109 e^- was excluded by a solvent mask. Modifications of **Δ-Br** show that the cavity within the macrocycle is occupied by halogenated solvents. Therefore, we conclude that the intrinsic channel is occupied by two disordered chloroform molecules per unit cell (118 e^- in total). The low boiling point of chloroform is expected to allow the use of the nanotube channel to incorporate small molecular guests, such as gases, for storage and separation applications.[12,13,27–31]

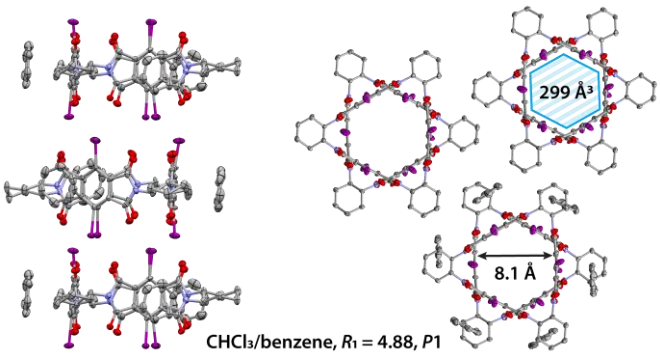

Fig. 3 SC-XRD structures of **Δ-I**. The columnar superstructure is displayed from side (left) and top (right) view. The solvent accessible void (CO_2 used as a probe) as well as the pore diameter is displayed. Color code: C, grey; O, red; N, blue; I, purple. Ellipsoids are shown at 50% probability and H and solvent molecules are omitted for clarity.

We explored the virtual porosity of the nanotubes by calculating the solvent accessible volume (Fig. 3). The size of the intrinsic pore could accommodate gases such as H_2, N_2, CO_2, and CH_4 (see SI, Fig S16 and Table S13). Additionally, the intrinsic void could be accessed by Li^+ ions, which makes **Δ-I** in combination with its multiple redox states[32] a promising material for reversible redox applications.

To gain a comprehensive understanding of the role of XBs on directing and stabilizing the supramolecular nanotubes, we investigated the nature and the strength of the involved XB interactions. We analysed the **Δ-I** dimer in the crystal unit cell with a combination of geometrical Hirshfeld surface (HS)[33], quantum theory of atoms in molecules (QT-AIM),[34] non-covalent interactions based on the reduced density gradient (NCI-RDG),[35] and model interaction energy analyses (Fig. 4).[36–39] By cataloguing all atom···atom distances closer than the sum of van der Waals radii in a histogram (Hirshfeld surface fingerprint[37], HS-FP) we observed that the predominant short contacts arise from H···H and C···H van der Waals forces (66.6%) resulting in a weak scaffold (Fig. 4A, blue and white regions). However, close distances between I···O (7.7%) and I···I (3.5%) atom pairs indicate the presence of XBs and type I halogen interactions stabilizing the structure (Fig. 4A, red dots). The electrostatic potential (ESP) map supports the presence of I···O XB motif with a σ-hole on the iodines and electron-rich oxygens (Fig. 4B). Additionally, we observe intramolecular polarization of the electron density in the iodine electron belt above the oxygen atom, which favours an intramolecular XB interaction.

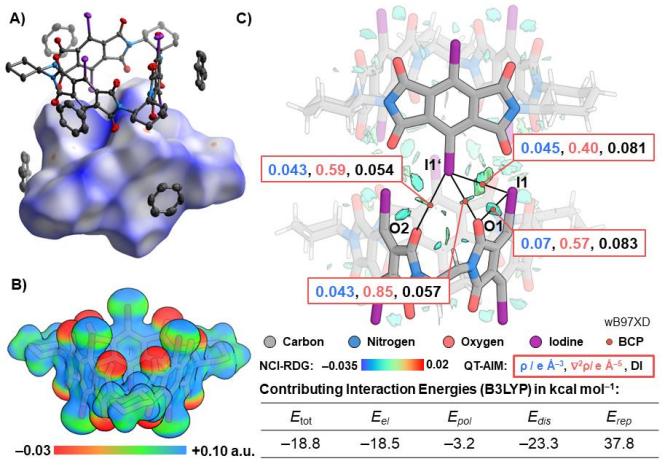

E_{tot}	E_{el}	E_{pol}	E_{dis}	E_{rep}
−18.8	−18.5	−3.2	−23.3	37.8

Fig. 4 Hirshfeld surface of **Δ-I** dimer and coordinated benzene molecules with the property d_{norm} color-coded onto it. Red, white, and blue areas indicate distances lower, commensurate or longer to the sum van der Waals radii; B) Electrostatic potential of **Δ-I** mapped onto an electron-density isosurface at 0.02 a.u.; C) NCI-RDG, QT-AIM and total interaction energy of the **Δ-I** dimer analyses**.** Bond paths and bond critical points (BCPs) are indicated with black lines and red dots, respectively. The electron density, and its Laplacian at BCPs as well as the delocalization index are shown for selected I I···I and I···O interactions. The individual contributions of E_{tot} are: electrostatic energy (E_{el}), polarization energy (E_{pol}), dispersion energy (E_{dis}) and repulsion energy (E_{rep}).

Inter- and intramolecular bond paths and their bond critical points (BCP) between iodine and/or oxygen atoms were analyzed by QT-AIM. Fig. 4C illustrates the BCPs formed by the O···I···O and I···I···O interactions. Despite the differences in the I···O bond lengths (see SI, Table S6), the electron density (ρ_{BCP}) and the delocalization index (DI) at the BCP are comparable between the two I…O interactions. However, the relatively low values of ρ_{BCP} and DI suggest that the interactions are weak in nature. Interestingly, a BCP with higher ρ_{BCP} and DI values describes the intramolecular I···O interaction, likely strengthened by the short distance between the atoms (3.3 Å). As a result, O1 polarizes the I1 atom and pushes its electron belt towards the I1' atom, strengthening the type I halogen interaction. The BCP for I(1)···I(1') displays a similar ρ_{BCP} value as for the I···O interactions but a higher DI of 0.081, indicating an increased electron pair exchange. The Laplacian of the electron density at the BCP ($\nabla^2\rho_{BCP}$) indicates that all bonding partners are closed-shell without significant charge transfer character.[40]

We visualized stabilizing and destabilizing interactions in the **Δ-I** dimer using NCI-RDG[35] and separated each contribution into attractive (Fig. 4C, blue), repulsive (red), and van der Waals interactions (green). NCI-RDG suggests that weak van der Waals forces hold the structure together (for the NCI-RDG surfaces of the destabilizing forces, see SI, Fig S14). These stabilization factors are mainly due to I···O XB and I···I interactions, as already demonstrated by the geometrical HS and QT-AIM analyses (Fig. 4, B).[41]

XBs are well-known to be electrostatic in nature[42], while type I halogen–halogen interactions are mainly dispersive[43] with low amounts of coulombic contributions[44]. The distance and orientation strongly affect the stabilization of both stronger C=O···I (2–5 kcal mol^{-1}) interaction and weaker type I I···I interactions (<1.5 kcal mol^{-1}).[38,45] We computed the total interaction energy (E_{tot} = –18.8 kcal mol^{-1}, Fig. 3C) from its individual scaled components, *i.e.*, electrostatic (E_{el}), polarization (E_{pol}), dispersion (E_{dis}), and repulsion energy (E_{rep}). In the **Δ-I** dimer, the suboptimal geometry reduces the C=O···I and I···I interactions decreasing their overall stabilization. Hence, in total the largest contributors are E_{el} and E_{dis}, with the latter being the dominant term per interaction.

The XB interactions clearly contribute to directing the growth of the supramolecular nanotubes from **Δ-I**, but their weak nature is likely not sufficient to stabilize the structure in the solid state alone. We note that the six benzene molecules coordinating with the electron-deficient PMDI aromatic cores likely contribute markedly to the nanotube stability. Indeed, attempts to grow **Δ-I** nanotubes using both non-aromatic and electron-poor aromatic solvents failed to yield any crystals or crystals of sufficient quality for XRD structure determination. Therefore, we believe that the solvent selection not only necessitates a non-competitive solvent for XB interactions but calls for the inclusion of a complementary stabilizing anti-solvent.

In conclusion, we successfully balanced the hydrogen bonding and halogen interactions to form a supramolecular nanotube from triangular PMDI macrocycles with only volatile $CHCl_3$ occupying the nanotube intrinsic void. This required to synthetically introduce iodine atoms to the macrocycle structure to geometrically disrupt the governing intermolecular hydrogen bonds, while strengthening halogen interactions. We explored the nature and strength of the underlying I···O and I···I interactions by geometrical Hirshfeld surface analysis and computations, which involved ESP, QT-AIM, NCI-RDG, and model energy analyses. Our strategy opens up possibilities to engineer halogen interactions in macrocycles to induce and direct growth of crystalline supramolecular nanotubes that could find applications as porous organic materials for gas storage and

separation, or as porous Li^+ ion acceptors required in research of organic rechargeable batteries.

The authors are grateful for the financial support from the European Research Council (ERC, Grant Agreement No. 949397), the Swiss National Science Foundation (SNSF, PZ00P2_174175, CRSK-2_190366), and the University of Bern.

Conflicts of interest

There are no conflicts to declare.

Notes and references

1 J. D. Watson and F. H. C. Crick, *Nature*, 1953, **171**, 737–738.
2 K. Yamada, H. Ihara, T. Ide, T. Fukumoto and C. Hirayama, *Chem. Lett.*, 1984, **13**, 1713–1716.
3 N. Nakashima, S. Asakuma and T. Kunitake, *J. Am. Chem. Soc.*, 1985, **107**, 509–510.
4 B. D. Harrison, T. M. A. Wilson and A. Klug, *Philos. Trans. R. Soc. Lond., B, Biol. Sci.*, 1999, **354**, 531–535.
5 M. Danial, C. My-Nhi Tran, P. G. Young, S. Perrier and K. A. Jolliffe, *Nat. Commun.*, 2013, **4**, 2780.
6 G. D. Pantoş, P. Pengo and J. K. M. Sanders, *Angew. Chem. Int. Ed.*, 2007, **46**, 194–197.
7 V. Percec, A. E. Dulcey, V. S. K. Balagurusamy, Y. Miura, J. Smidrkal, M. Peterca, S. Nummelin, U. Edlund, S. D. Hudson, P. A. Heiney, H. Duan, S. N. Magonov and S. A. Vinogradov, *Nature*, 2004, **430**, 764–768.
8 S. Hecht and A. Khan, *Angew. Chem. Int. Ed.*, 2003, **42**, 6021–6024.
9 M. R. Ghadiri, J. R. Granja, R. A. Milligan, D. E. McRee and N. Khazanovich, *Nature*, 1993, **366**, 324–327.
10 A. Casnati, R. Liantonio, P. Metrangolo, G. Resnati, R. Ungaro and F. Ugozzoli, *Angew. Chem. Int. Ed.*, 2006, **45**, 1915–1918.
11 C. T. Kresge, M. E. Leonowicz, W. J. Roth, J. C. Vartuli and J. S. Beck, *Nature*, 1992, **359**, 710–712.
12 A. Chaix, G. Mouchaham, A. Shkurenko, P. Hoang, B. Moosa, P. M. Bhatt, K. Adil, K. N. Salama, M. Eddaoudi and N. M. Khashab, *J. Am. Chem. Soc.*, 2018, **140**, 14571–14575.
13 K. Jie, M. Liu, Y. Zhou, M. A. Little, S. Bonakala, S. Y. Chong, A. Stephenson, L. Chen, F. Huang and A. I. Cooper, *J. Am. Chem. Soc.*, 2017, **139**, 2908–2911.
14 J. M. Van Raden, E. J. Leonhardt, L. N. Zakharov, A. Pérez-Guardiola, A. J. Pérez-Jiménez, C. R. Marshall, C. K. Brozek, J. C. Sancho-García and R. Jasti, *J. Org. Chem.*, 2020, **85**, 129–141.
15 Z. Liu, J. Sun, Y. Zhou, Y. Zhang, Y. Wu, S. K. M. Nalluri, Y. Wang, A. Samanta, C. A. Mirkin, G. C. Schatz and J. F. Stoddart, *J. Org. Chem.*, 2016, **81**, 2581–2588.
16 Z. Liu, G. Liu, Y. Wu, D. Cao, J. Sun, S. T. Schneebeli, M. S. Nassar, C. A. Mirkin and J. F. Stoddart, *J. Am. Chem. Soc.*, 2014, **136**, 16651–16660.
17 Y. Wu, S. K. M. Nalluri, R. M. Young, M. D. Krzyaniak, E. A. Margulies, J. F. Stoddart and M. R. Wasielewski, *Angew. Chem. Int. Ed.*, 2015, **54**, 11971–11977.
18 D. Cao, M. Hong, A. K. Blackburn, Z. Liu, J. M. Holcroft and J. F. Stoddart, *Chem. Sci.*, 2014, **5**, 4242–4248.
19 S. Garain, S. Naz Ansari, A. Ajayan Kongasseri, B. C. Garain, S. K. Pati and S. J. George, *Chem. Sci.*, 2022, **13**, 10011–10019.
20 J. Gawroński, M. Brzostowska, K. Gawrońska, J. Koput, U. Rychlewska, P. Skowronek and B. Nordén, *Chem. Eur. J.*, 2002, **8**, 2484–2494.
21 D. Wang and Y. Zhao, *Angew. Chem. Int. Ed.*, 2023, **62**, e202217903.
22 M. J. Kamlet and R. W. Taft, *J. Am. Chem. Soc.*, 1976, **98**, 377–383.
23 R. W. Taft and M. J. Kamlet, *J. Am. Chem. Soc.*, 1976, **98**, 2886–2894.
24 H.-H. Huang and T. Šolomek, *Chimia*, 2021, **75**, 285–290.
25 T. Šolomek, N. E. Powers-Riggs, Y.-L. Wu, R. M. Young, M. D. Krzyaniak, N. E. Horwitz and M. R. Wasielewski, *J. Am. Chem. Soc.*, 2017, **139**, 3348–3351.
26 H.-H. Huang, K. S. Song, A. Prescimone, A. Aster, G. Cohen, R. Mannancherry, E. Vauthey, A. Coskun and T. Šolomek, *Chem. Sci.*, 2021, **12**, 5275–5285.
27 L.-L. Tan, H. Li, Y. Tao, S. X.-A. Zhang, B. Wang and Y.-W. Yang, *Adv. Mater.*, 2014, **26**, 7027–7031.
28 B. Shi, L. Shangguan, H. Wang, H. Zhu, H. Xing, P. Liu, Y. Liu, J. Liu and F. Huang, *ACS Mater. Lett.*, 2019, **1**, 111–115.
29 L.-L. Tan, Y. Zhu, H. Long, Y. Jin, W. Zhang and Y.-W. Yang, *Chem. Commun.*, 2017, **53**, 6409–6412.
30 P. Wang, Y. Wu, Y. Zhao, Y. Yu, M. Zhang and L. Cao, *Chem. Commun.*, 2017, **53**, 5503–5506.
31 B. Moosa, L. O. Alimi, A. Shkurenko, A. Fakim, P. M. Bhatt, G. Zhang, M. Eddaoudi and N. M. Khashab, *Angew. Chem. Int. Ed.*, 2020, **59**, 21367–21371.
32 D. J. Kim, K. R. Hermann, A. Prokofjevs, M. T. Otley, C. Pezzato, M. Owczarek and J. F. Stoddart, *J. Am. Chem. Soc.*, 2017, **139**, 6635–6643.
33 M. A. Spackman and D. Jayatilaka, *CrystEngComm*, 2009, **11**, 19–32.
34 R. F. W. Bader, *Acc. Chem. Res.*, 1985, **18**, 9–15.
35 E. R. Johnson, S. Keinan, P. Mori-Sánchez, J. Contreras-García, A. J. Cohen and W. Yang, *J. Am. Chem. Soc.*, 2010, **132**, 6498–6506.
36 HS analysis revealed the presence of two non-equivalent C=O···I bonding interactions (rO···I = 3.4 Å and 3.6 Å, ∢ = 103° and 120°) shorter than the sum of van der Waals radii.
37 P. R. Spackman, M. J. Turner, J. J. McKinnon, S. K. Wolff, D. J. Grimwood, D. Jayatilaka and M. A. Spackman, *J. Appl. Crystallogr.*, 2021, **54**, 1006–1011.
38 K. E. Riley, J. S. Murray, J. Fanfrlík, J. Řezáč, R. J. Solá, M. C. Concha, F. M. Ramos and P. Politzer, *J. Mol. Model.*, 2011, **17**, 3309–3318.
39 M. J. Turner, S. Grabowsky, D. Jayatilaka and M. A. Spackman, *J. Phys. Chem. Lett.*, 2014, **5**, 4249–4255.
40 R. F. W. Bader and H. Essén, *J. Chem. Phys.*, 1984, **80**, 1943–1960.
41 O···H interactions were observed, which were previously reported in the downfield shift with increasing ring size and decreasing overlap in 1H NMR spectroscopy (NMR) of these compounds (see Ref. 19 and 30). An attractive intramolecular O···O contact isosurface can be seen, but its explanation remains unknown.
42 T. T. T. Bui, S. Dahaoui, C. Lecomte, G. R. Desiraju and E. Espinosa, *Angew. Chem. Int. Ed.*, 2009, **48**, 3838–3841.
43 A. Saha, S. A. Rather, D. Sharada and B. K. Saha, *Cryst. Growth Des.*, 2018, **18**, 6084–6090.
44 F. F. Awwadi, R. D. Willett, K. A. Peterson and B. Twamley, *Chem. Eur. J.*, 2006, **12**, 8952–8960.
45 M. A. A. Ibrahim, R. R. A. Saeed, M. N. I. Shehata, M. N. Ahmed, A. M. Shawky, M. M. Khowdiary, E. B. Elkaeed, M. E. S. Soliman and N. A. M. Moussa, *Int. J. Mol. Sci.*, 2022, **23**, 3114.